

Ryan A. Howard

e-mail: rhoward@imvprojects.com

Joshua M. Rosvold

Research Associate
e-mail: jmrosvol@ucalgary.ca

Shon P. Darcy

e-mail: sdarcy@ucalgary.ca

David T. Corr

e-mail: corrd@rpi.edu

Nigel G. Shrive

Professor
e-mail: shrive@ucalgary.ca

Department of Civil Engineering,
Schulich School of Engineering,
University of Calgary,
c/o Joint Injury and Arthritis Research Group,
3330 Hospital Drive,
Calgary, Alberta, Canada T2N 4N1

Janet E. Tapper

e-mail: janet.tapper@med.ucalgary.ca

Janet L. Ronsky

Professor and CRC in Biomedical Engineering
e-mail: jlronsky@ucalgary.ca

Department of Mechanical and Manufacturing
Engineering,
Schulich School of Engineering,
University of Calgary,
c/o Joint Injury and Arthritis Research Group,
3330 Hospital Drive,
Calgary, Alberta, Canada T2N 4N1

Jillian E. Beveridge

e-mail: jill.beveridge@ucalgary.ca

Linda L. Marchuk

Research Associate
e-mail: marchuk@ucalgary.ca

Cyril B. Frank

Professor and Division Head,
Orthopaedic Surgery
e-mail: cfrank@ucalgary.ca

Department of Surgery,
University of Calgary,
c/o Joint Injury and Arthritis Research Group,
3330 Hospital Drive,
Calgary, Alberta, Canada T2N 4N1

Reproduction of In Vivo Motion Using a Parallel Robot

Although alterations in knee joint loading resulting from injury have been shown to influence the development of osteoarthritis, actual in vivo loading conditions of the joint remain unknown. A method for determining in vivo ligament loads by reproducing joint specific in vivo kinematics using a robotic testing apparatus is described. The in vivo kinematics of the ovine stifle joint during walking were measured with 3D optical motion analysis using markers rigidly affixed to the tibia and femur. An additional independent single degree of freedom measuring device was also used to record a measure of motion. Following sacrifice, the joint was mounted in a robotic/universal force sensor test apparatus and referenced using a coordinate measuring machine. A parallel robot configuration was chosen over the conventional serial manipulator because of its greater accuracy and stiffness. Median normal gait kinematics were applied to the joint and the resulting accuracy compared. The mean error in reproduction as determined by the motion analysis system varied between 0.06 mm and 0.67 mm and 0.07 deg and 0.74 deg for the two individual tests. The mean error measured by the independent device was found to be 0.07 mm and 0.83 mm for the two experiments, respectively. This study demonstrates the ability of this system to reproduce in vivo kinematics of the ovine stifle joint in vitro. The importance of system stiffness is discussed to ensure accurate reproduction of joint motion. [DOI: 10.1115/1.2768983]

Keywords: knee, ligament, kinematics, gait, robotics

Introduction

Osteoarthritis (OA) is a degenerative joint disease that affects

more than 80% of people over the age of 55 [1]. In some cases, OA is thought to be caused by the changes in joint loading and stability following ligament injury and/or reconstruction [2]. Thus, there is an interest in the mechanical influences on tissues that lead to OA. Changes in mechanical loading of the joint are speculated to contribute to the biological changes associated with the development of OA. Currently, as the factors associated with the

Contributed by the Bioengineering Division of ASME for publication in the JOURNAL OF BIOMECHANICAL ENGINEERING. Manuscript received August 5, 2005; final manuscript received May 1, 2007. Review conducted by Frank Yin.

development of OA are not well understood, only the symptoms are treated.

Surgical reconstruction of the ligament is frequently performed following knee ligament injury in an attempt to restore normal joint function and to prevent or impede the development of OA. While anterior cruciate ligament (ACL) reconstruction can subjectively restore joint stability, it has not been established whether ACL reconstruction definitively retards the progression of OA [3–6]. It is necessary to understand the mechanics of the normal joint in order to address the problem of post-injury joint degeneration. Such knowledge can be used to relate changes in the mechanics of joint structures to biological changes. The ultimate goal is to develop surgical techniques and treatments that are able to diminish or prevent the clinically observed osteoarthritic degeneration of the joint.

Many studies have attempted direct measurement of loading in the knee structures with limited success. Most commonly, joint tissue strain measurements have been recorded using Hall effect strain transducers [7], and extensometers [8], while force measurements have been attempted through the use of buckle transducers [9], arthroscopically implantable force probes [10], or pressure transducers [11] implanted onto the structure of interest. These techniques are highly invasive, and thus, the results may be influenced by the surgery and/or the mechanical interference caused by the implanted sensor. Strain gauges measure at best the local strain at the surface. Due to the complex bundled structure of ligaments, such localized measurements may not be indicative of the global strain in the structure [12].

Recent technological advances in the field of industrial robotics have allowed increasingly complex loading regimes to be applied to various joints and tissues. A unique application of hybrid control pioneered by Fujie, Rudy, and Woo as well as various other researchers allows the estimation of tissue loads and their functions during passive joint motion and applied in vitro loads [13–20].

The purpose of the study described here was to develop and evaluate a technique for the robotic reproduction of previously measured subject-specific in vivo motion based on spatial referencing, a parallel robot, and custom software. Various methods for determining dynamic in vivo joint kinematics have been developed based on fluoroscopy and motion analysis with marker cluster approaches [21–23]. However, the method of Tapper et al. [24], based on optical motion analysis, was used as it provided both the necessary positional accuracy and external rigid markers that could be referenced with respect to anatomical landmarks, joint structures, and the robot global coordinates. A unique 6 degree-of-freedom (DOF) parallel manipulator (R-1000, PR-SCo, Hampton, NH) was used to reproduce the recorded three-dimensional (3D) motion.

Methods

In Vivo Kinematic Measurements. Kinematics of the stifle joint of two ($n=2$) adult sheep were measured using stainless steel plates implanted on the femur and tibia, with rigid marker tetrads mounted on these plates during testing as per the method of Tapper et al. [24]. Three-dimensional spatial positions of the four tibial and four femoral reflective markers were measured during level treadmill walking (2 mph) using a four-camera (Falcon hi-resolution infrared cameras, 120 Hz) video based motion analysis system (Expert Vision, Motion Analysis Corporation, Santa Rosa, CA). All animal surgeries and testing were approved by the University of Calgary Animal Care Committee and comply with the guidelines of the Canadian Council on Animal Care. 3D kinematics were measured for approximately 230 strides beginning and ending at hoof strike. The mean single point error for in vivo motion was $0.29 \text{ mm} \pm 0.19 \text{ mm}$. Data were smoothed using a generalized cross-validation filter using cubic splines and a low-pass cut-off frequency of 6 Hz. The global positions of the four

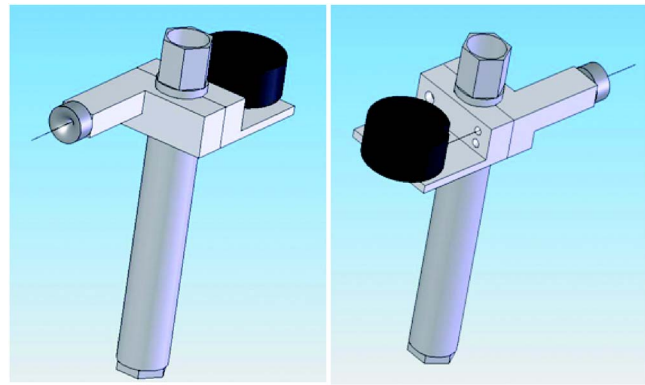


Fig. 1 Transducer assembly on the femoral post

tibial and four femoral markers were normalized to 101 positions, corresponding to 0–100% gait cycle. Immediately following the in vivo motion analysis measurements, the animal was euthanized by intravenous injection (Euthanyl, Bimeda-MTC, Cambridge, ON, CND), and the leg harvested and dissected of all surrounding soft tissue.

The relative coordinate transformations between the global coordinate system and the anatomical coordinate systems were determined using a singular value decomposition method [25]. This procedure required the coordinates of each marker in both the global coordinate system (GCS) of the motion analysis and in its respective anatomical coordinate systems in the tibia (TCS) or femur (FCS) in order to calculate the global to anatomical transformation. The anatomic coordinate systems are created by aligning the z -axis with the long axis of the bone, directed in the superior sense. The y -axis is orthogonal to a plane created from the z -axis and a line connecting the insertions of the MCL and the LCL. The x -axis completes the right-hand frame and the origin is located at the center of the ACL insertion. Coordinate transformations determined from the GCS to the anatomical coordinate systems (TCS, FCS) are represented as $[T]_{GCS}^{TCS}$ and $[T]_{GCS}^{FCS}$. The gait cycle is described by 101 transformations from the TCS to the FCS.

A representative 100 strides were kept from the initial 230 and a least-squares method was used to determine the median stride.

Independent Measurement. A cable transducer (50.8 mm maximum travel, 0.012 mm resolution, Series 170-0161-2N, Space Age Control, Palmdale, CA) was used to measure the distance between the tops of the two sets of posts attached to the plates in the femur and tibia. This transducer's small size, together with the flexibility provided by the cable, make it well suited for this application. Custom mounts were designed to fix the transducer onto the marker posts, and the posts were modified to accept these mounts (Figs. 1 and 2).

In order to ensure the safety of the animal, as well as to avoid damaging the sensor, a mechanism was designed so that if the cable reached the end of its stroke, a magnet would release the cable, thereby preventing damage to the transducer. This mechanism is shown in Fig. 2. The excess cable was fixed in a specially designed clamp to keep it safely away from the animal.

Robot. The in vivo motion was reproduced using a 6 DOF parallel robot (accuracy: 0.050 mm, R-1000, PR-SCo, Hampton, NH). The robot design is based on a Stewart Platform, whereby instead of the leg lengths being actuated, six fixed length legs are actuated about a circular track. The change in relation between the bases of the legs allows the robot to achieve 6 degrees of-freedom motion. With this particular robot, ± 720 deg rotation of the end effector can be achieved about the central axis of the machine and ± 14 deg about the horizontal axes. The legs are attached by ball

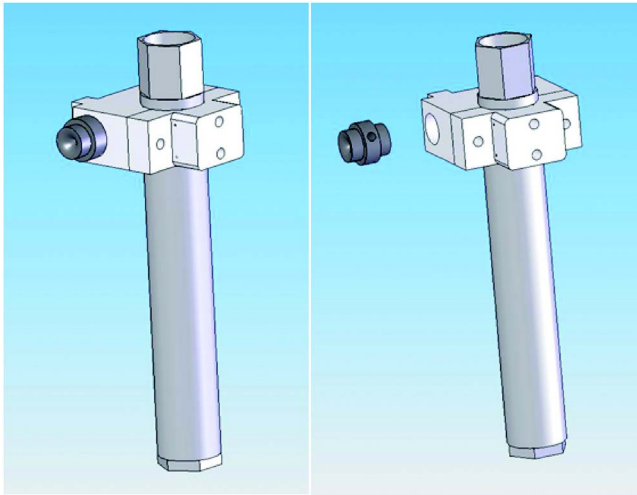


Fig. 2 Cable fixing system and safety release on the tibial post

joints to both the end effector and the rotating bases. This parallel design allows for increased stiffness and accuracy over conventional serial manipulators, where any deflection in joints and members is propagated through the robot [26].

Load Floor. Reproduction of the measured motion is based on the concept of holding the tibia in a fixed position, and using the robot to move the femur through its motion, relative to the tibia. To reproduce the motion with fidelity requires accuracy of the robot and stiffness of both the robot and the tibial supports. Stiffness is required so that neither the robot nor the support deform under the joint loads that develop, such that the bones are no longer in the position relative to each other, as measured in vivo. Thus, while the parallel robot is designed to be stiff, the tibial supports must also be stiff. Consequently, a custom load floor was designed along with a 6 degrees-of-freedom tibial fixation pot, as can be seen in Fig. 3. A high performance, self-leveling concrete (Agilia) was used with a grid of 100 mm by 100 mm of 50 M grade reinforcing steel. This structure was constructed on top of a rubber mat to isolate the floor from vibrations. Three-quarter inch stainless steel plates were then fixed on the top and frontmost sides of the concrete with a modular bolt hole pattern of 250 mm square to accommodate the rigid attachment of the robot base, the tibial fixture, and other peripheral devices. The robot is rigidly

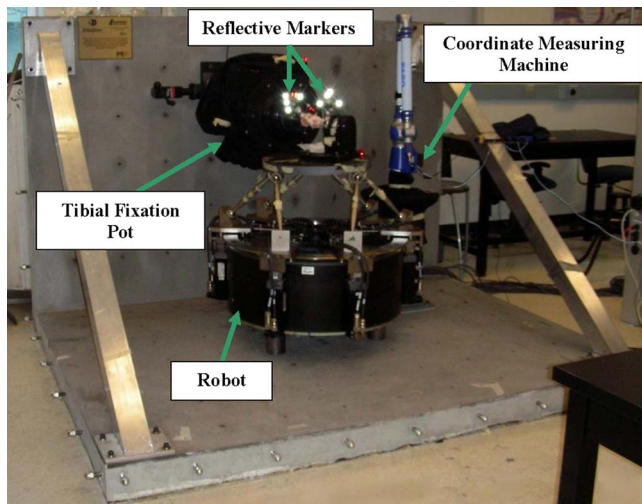


Fig. 3 Custom designed load floor and tibial fixation pot

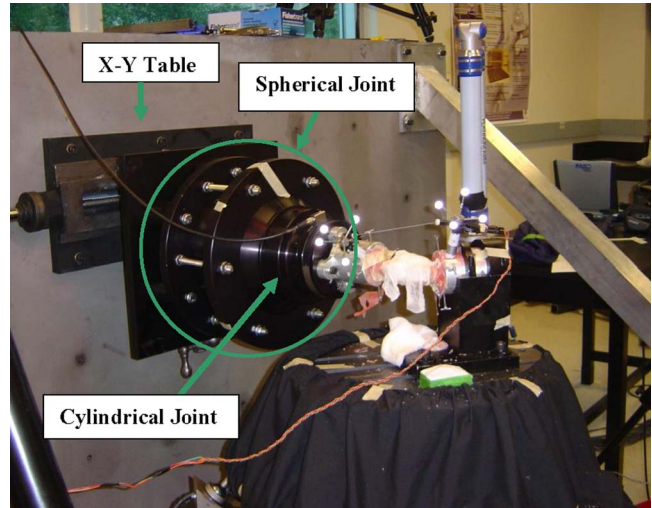


Fig. 4 Tibial fixation pot

bolted to the lower floor.

A closer view of the tibial fixation pot is provided in Fig. 4. This fixation system employs an X-Y table at its base on the side wall of the load floor and a ball joint. A cylindrical joint was machined inside the ball on which a universal force/moment sensor (Omega 160, ATI Industrial Automation Apex, NC) is attached, followed by the tibial pot.

The stiffness of this tibial fixation system is listed in Table 1. Load was applied to the end of the tibial pot and the resulting deformation recorded.

Joint Landmark and Marker Pretest Digitization. All marker and surface referencing was performed with a portable coordinate measuring machine (CMM) (single-point accuracy: 0.025 mm, FaroArm Platinum, Faro Technologies, Lake Mary, FL). The CMM configuration (6 DOF and 1.8 m range) enabled access to the marker systems and joint for the pretest digitizations, as well as for subsequent measurements, when mounted on the robot. The joint was fixed in a rigid frame and care was taken to ensure that the marker tetrads and posts were not bumped or removed during this process. The coordinates of the marker sets were determined with the CMM by referencing the individual markers as spheres. The CMM was also used to measure the positions of the markers relative to anatomical landmarks, to enable calculation of the anatomical femoral (FCS) and tibial (TCS) coordinate systems [24].

Specimen Mounting. Following digitization, the femur and tibia were sectioned proximally and distally, respectively, to the joint, and the tibia was cemented into a custom aluminum bone pot using polymethylmethacrylate (PMMA). The tibial pot assembly was then mounted on the tibial fixture system. The initial joint position was such that the sagittal plane was roughly aligned with the surface of the robot end effector. This position also aligned the flexion-extension axis, the primary axis of rotation, with the central axis of the robot. To verify that the path of motion of the robot end effector would occur within the envelope of motion of the

Table 1 Stiffness of the tibial fixation system

Loading type	Stiffness
Axial compression	34,290 N/mm
Axial tension	266,160 N/mm
Bending vertical	43,330 N/mm
Bending lateral	17,400 N/mm
Torsion	15,080 N m/°

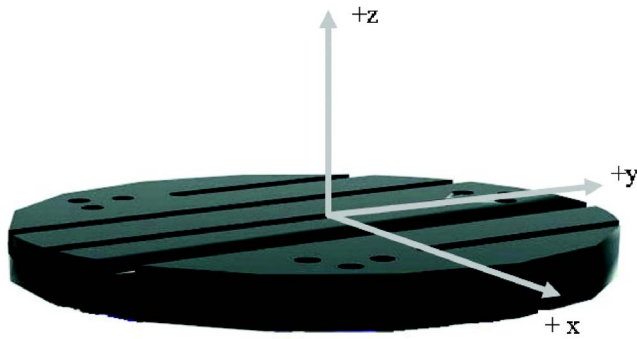


Fig. 5 Robot global coordinates (RGCs)

robot, the paths of robotic motion were calculated prior to cementing the femur in its pot. The femur was nondestructively pinned within the custom mounting pot in an arbitrary position relative to the robot end effector at the zero pose orientation tetrad markers digitized and robot paths of motion calculated.

In the case where the required motion was outside of the robot's range, the positions of the tibial and/or femoral pots were modified, the mounting pots were reclamped and the femur repinned. The spatial referencing procedure was repeated until a joint position providing path within the robot's working space was found. The femur was then cemented into the femoral pot in this final position using PMMA. The referencing procedure was repeated for a final time following cement curing. All joint tissues were irrigated with phosphate buffered saline solution throughout testing to minimize soft tissue desiccation.

Calculation of Robot Kinematics. Determination of the robotic path of motion that replicates in vivo 3D kinematics requires referencing the robot's global coordinate system to that of the reflective markers. The CMM was used to determine these coordinate transformations. Given the high level of accuracy desired for this system, the location of the origin of the robot global coordinate system (RGCS) had to be determined accurately. Using the CMM, RGCS was referenced by measuring the position of a precision ball rigidly affixed to the end effector in several different robot positions. The centroid of this ball were measured at ± 14 deg of rotation about both the x -axis and the y -axis of the robot's global coordinate system, as well as 30 deg increments about the global z -axis. These measurements were fit to a sphere whose origin represents that of the RGCS. A plane parallel to the XZ -plane was defined by measuring the ball at ± 10 , 20, and 45 mm translations in the x - and z -directions. The vector normal to the XZ -plane defined the direction of the y -axis of the RGCS. The x -axis was defined by measuring the intersection of the XZ - and the XY -planes where the XY -plane was found in a similar manner to the XZ -plane, using robot positions in the y -direction rather than the z -direction. The z -axis completes the right-hand frame, and the approximate location and orientation can be seen in Fig. 5.

Replication of the in vivo joint positions throughout the range of motion by the robot end effector required determination of positions of the femoral and tibial markers in their final fixed location relative to the RGCS. These coordinate transformations were used with the 101 in vivo marker positions from the median gait cycle to calculate the 101 positions of the dynamic robot coordinate system (RCS) embedded in the robot end effector (Fig. 6). This robot positioning process involves applying the singular value decomposition method [25] to calculate the two 4×4 homogeneous transformation matrices from the RGCS to the TCS in its arbitrary fixed position(s), (TCS), and from the RGCS to the FCS in its arbitrary fixed position(s), (FCS). These calculations were based on both the previously measured position of the four

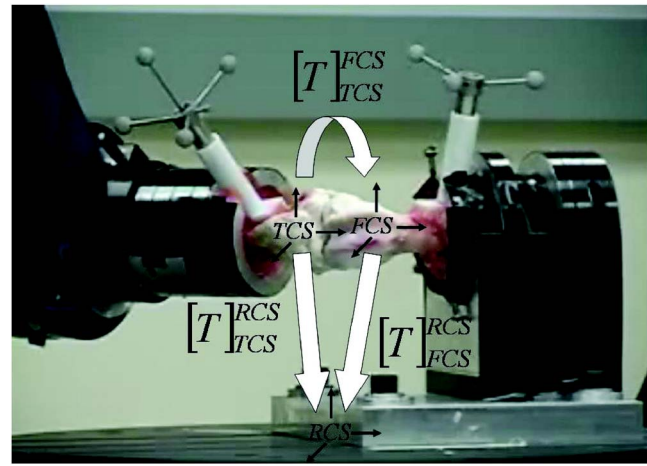


Fig. 6 4×4 homogeneous transformation matrices describing the position of the FCS relative to the TCS, FCS relative to RCS

femoral and four tibial markers relative to the FCS and TCS, respectively, as well as the position of the four femoral and four tibial markers relative to the RGCS.

The calculated paths were then used to find the positions of the RCS relative to the TCS necessary to reproduce the in vivo positions of the RCS relative to the TCS, as outlined in the flowchart in Fig. 7. The moving position of the robot end effector was defined as the position of the embedded RCS relative to the stationary RGCS. In order to relate the 101 in vivo positions of the RCS to the RGCS for each path, the 101 RCS positions relative to the RGCS were calculated based on the transformations from the RCS to the calculated in vivo positions of the RCS for each path:

$$[T]_{RGCS}^{RCS} = ([T]_{TCS}^{RGCS})^{-1} * [T]_{TCS}^{RCS} \quad (1)$$

For the specific robotic manipulator used, the software interface uses cardinal angles and translations along an orthogonal coordinate system (RGCS). The three rotations were performed in the user defined order of yaw (about the z -axis of the RGCS), pitch (about the y -axis of the RGCS), and roll (about the x -axis of the RGCS). The largest kinematic rotation occurs in flexion exten-

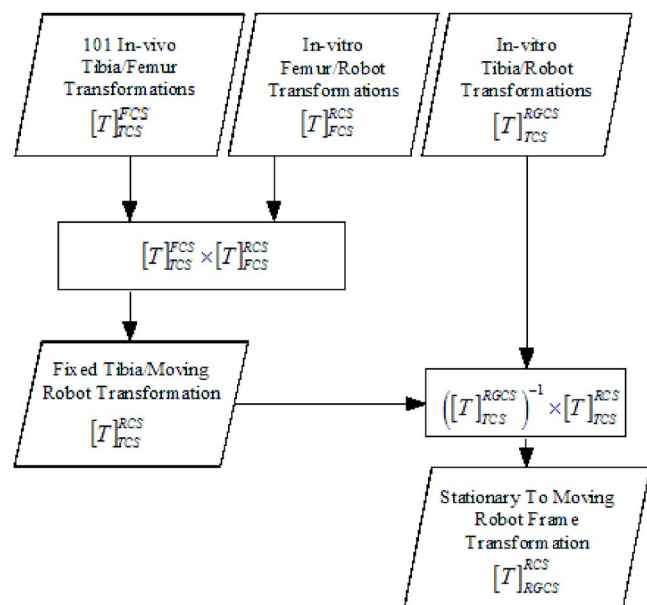


Fig. 7 Flowchart for robot end-effector path determination

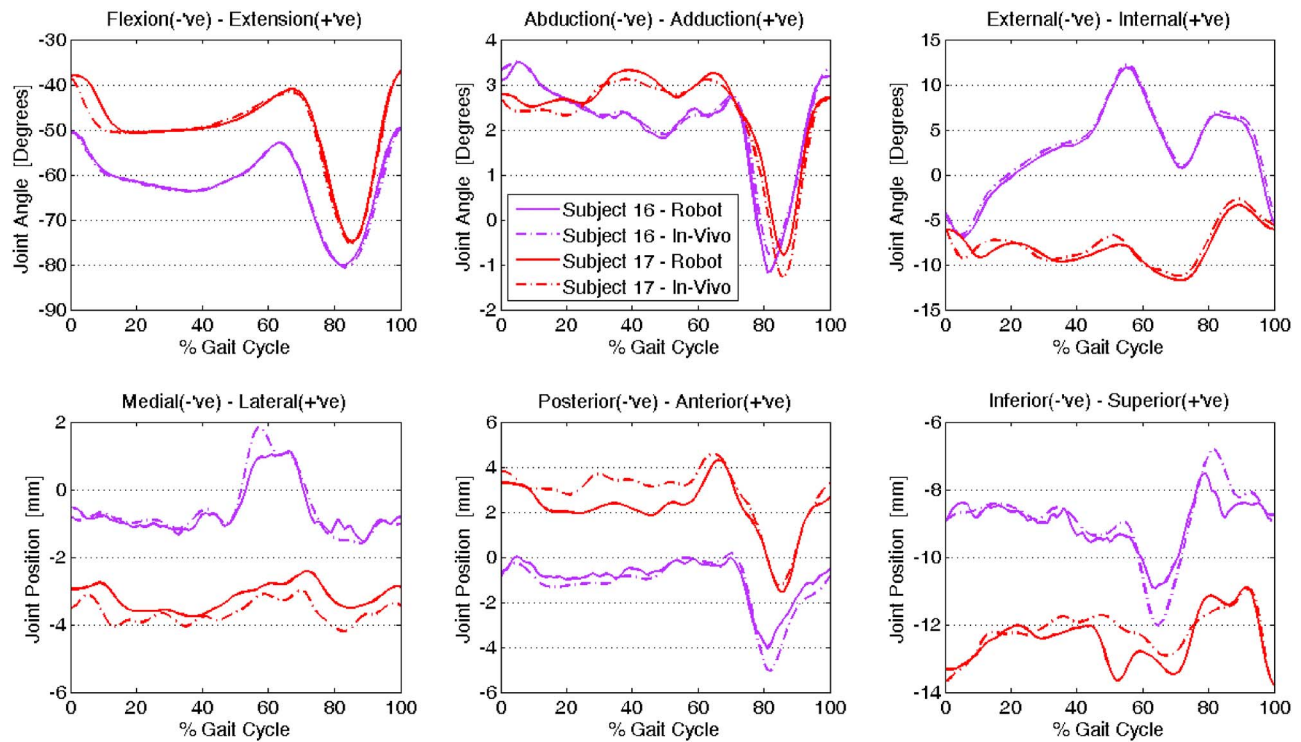


Fig. 8 In vivo and in vitro joint motion

sion, which was mounted approximately about the z -axis of the robot. Consequently, yaw was selected as the first rotation to be executed in order to minimize error in the rotation sequence. The calculated transformation matrices from the RGCS to the 101 in vivo positions of the RCS were used to solve for the x, y, z translations and rotations for the 101 in vivo positions of the end effector for each path using the method described by Slabaugh [27]. Each path was then manually evaluated in terms of fit within the 6 DOF envelope of motion of the manipulator.

Execution of Paths. Following the calculation of the robotic paths of motion, the femur was initially moved by the manipulator from its arbitrarily mounted position to the closest position in the in vivo path. Joint loads were recorded during this move to ensure that no abnormally large loads were applied to the joint. The femur was then moved to the beginning of the median path, corresponding to hoof strike. Next, the median path was applied at 1/20th of in vivo speed and the resulting motion and load recorded.

In vitro Kinematics Measurements. Motion was recorded in a similar manner to the in vivo kinematics except a six-camera setup was used around the robot apparatus to ensure that the markers could be properly seen by the camera system (mean error = $0.31 \text{ mm} \pm 0.15 \text{ mm}$). Force and moment data were also recorded during motion using a synchronizing signal issued from the robot.

Due to mechanical limitations of the robot, variation of the time taken between positions occurred. A spline function was used to normalize the number of data points between each commanded position. These data could then be directly compared with the in vivo motion.

Results

Data from the motion analysis system were recorded and following protocol, smoothed using the same filter as was used for

the in vivo kinematics, except with a 0.3 Hz cut-off frequency. The anatomical motion of the joint for both trials can be seen in Fig. 8.

The discrepancy between the in vivo motion and what was produced on the robot is shown in Fig. 9.

Data from the independent measuring device are shown in Fig. 10. It should be noted that due to the different orientations of the sensor, there is not expected to be any strong correlation between the displacements recorded for the two animals.

The difference between the in vivo readings and those produced in vitro can be seen in Fig. 11.

A summary of the difference between in vivo and in vitro motion is presented in Table 2.

To determine the deformation of the tibia during motion, a machined cube was affixed to the tibial pot (measuring cube repeatability = 0.08 mm). Under a compressive load of 3.5 kN (approximately three times as large as what was seen during robot motion) applied axially to the tibial pot, the tibial fixture deformed 0.169 mm in the direction of the applied load.

Discussion

The motion of the femoral markers relative to the tibial markers is based on in vivo measurements. To reproduce this motion in vitro, either (a) the deformations of the manipulator and frame under the loads that develop have to be accounted for by altering the path imposed by the manipulator appropriately, or (b) the manipulator and frame must deform negligibly under load. The mathematical method used to calculate the in vivo path of motion assumes infinite rigidity of both the external load frame used to fix the tibia distal to the implanted markers, and the robotic end effector used to manipulate the femur distal to the implanted markers. To satisfy this assumption, a custom tibial load frame was designed and manufactured. While this frame allowed motion of the potted tibia-femur complex in 6 DOF for position optimization of the joint relative to the end effector during mounting, the frame also ensured stiff fixation of the tibia when the load frame joints

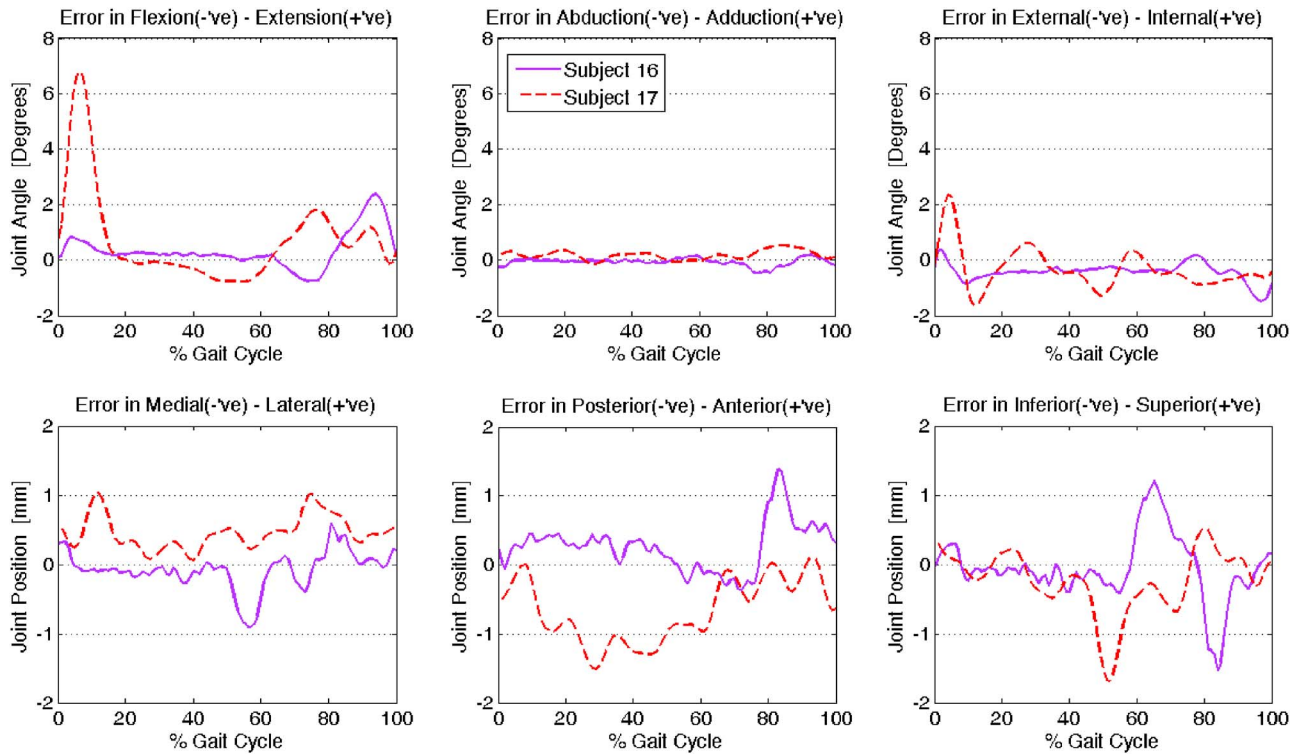


Fig. 9 Error in robot reproduction of in vivo motion

were “locked.” The stiffness and accuracy of the robotic manipulator used was also maximized through use of a parallel configuration, which offers the inherent benefits of “greater stiffness, higher payload/weight ratio, reduced inertia, and higher precision” [26] when compared to commercially available serial manipulators. The tradeoff for this increase in performance is that the range of motion is smaller. Given the measurements of the deformation of the tibial pot under load, it is reasonable to state that tibial pot deformation would be negligible under physiologic, in vivo loading. Further, this deformation could not be detected by the motion analysis system, since it is within the accuracy measurements of that system. This minimal deformation is crucial to ensure that the motion is accurately reproduced.

The error of this system’s reproduction of in vivo motion, as presented in Table 2 can be attributed to several factors. As pre-

viously mentioned, the stiffness of the system significantly affects its ability to position the joint accurately under load. Also, there are transient effects resulting from the timing of the system. In the flexion-extension plot in Fig. 8, the robot motion can be seen to lag behind the in vivo motion from 0–10% for Sheep 17. So, while the robot is moving to the correct position, it may not be at the correct position at the correct time. This is a mechanical limitation of the robot mainly due to its inability to reach the infinite acceleration required to step into gait motion instantaneously. There has been an attempt to account for this by normalizing the data, but perhaps the number of intervals that are taken throughout the total path (100) needs to be increased. Further errors that can be propagated through the system are the CMM measurements of both the RGCS and the marker positions. Last, the accuracy of the motion analysis system needs to be considered.

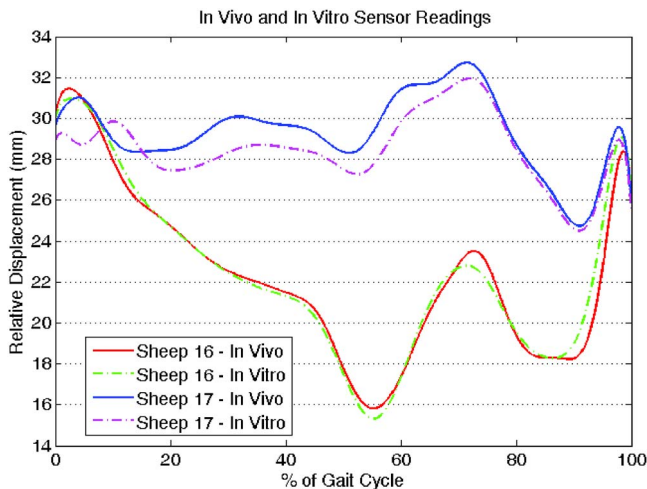


Fig. 10 In vivo and in vitro sensor readings

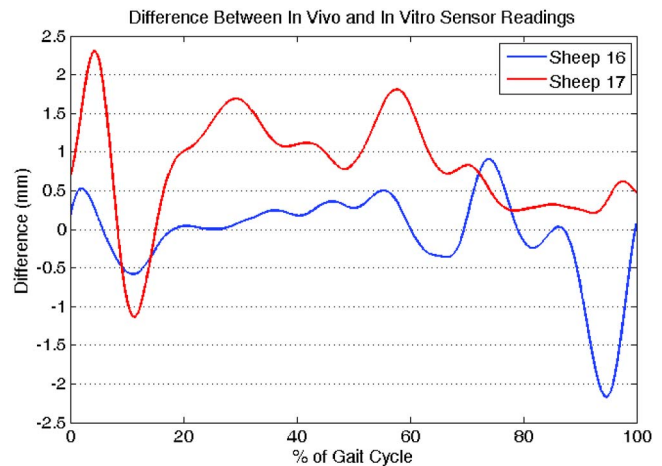


Fig. 11 Difference between in vivo and in vitro sensor readings

Table 2 Summary of differences between in vivo and in vitro readings

Measurement	Sheep 16		Sheep 17	
Displacement	-0.07	+/- 0.58 mm	0.83	+/- 0.66 mm
Flexion-Extension	0.34	+/- 0.66 deg	0.74	+/- 1.67 deg
Adduction-Abduction	-0.07	+/- 0.14 deg	0.18	+/- 0.16 deg
Internal-External	-0.43	+/- 0.33 deg	-0.33	+/- 0.74 deg
Medial-Lateral	-0.08	+/- 0.28 mm	0.46	+/- 0.24 mm
Posterior-Anterior	0.26	+/- 0.35 mm	-0.67	+/- 0.46 mm
Superior-Inferior	-0.06	+/- 0.48 mm	-0.24	+/- 0.46 mm

Conclusions

Using two sheep in this study, the mathematical method developed for reproducing in vivo 3D kinematics of the stifle joint using a parallel manipulator was verified. System stiffness is an important component of the method.

Once the kinematics and kinetics of the normal, uninjured joint are understood, this method will be employed to observe and quantify how these kinetics change following connective tissue injury. Ultimately, the knowledge provided can be used to relate the changes in joint mechanics to the osteoarthritic changes that develop following injury, as well as providing a model for the improvement of surgical reconstruction techniques in terms of their ability to restore not only normal joint kinematics, but also the kinetics.

Acknowledgment

We would like thank S. Adeeb, P. Goldsmith, and PRSCo for their contribution to the development of the robotic testing system. The following people were instrumental in the design and construction of the load floor: B. Storey, R. Scorey, T. Quinn, G. Johnson, S. Saad, P. Lavoie, T. Williams, D. Fantini, J. Sabourin, and C. Stern. We would also like to express our appreciation to C. Sutherland and L. Jaques for their contributions with our animal care and training. Last, we would like to thank the following agencies for funding this research: AHFMR, AIF, CCIT, CFI, CIHR, Ellis Don, Ernst and Young, GEOIDE, Lafarge, NCE, NSERC, and TAS.

References

- [1] Schwartz, S. T., and Zimmermann, B., 1999, "Update on Osteoarthritis," *Med. Health R. I.*, **82**(9), pp. 321–324.
- [2] Tapper, J. E., Barnsdale, C., Funakoshi, Y., Hariu, M., Sutherland, C., Thornton, G. M., Ronsky, J. L., Shrive, N. G., and Frank, C. B., 2004, "Evidence Supporting a New Hypothesis for the Development of Osteoarthritis," *Transactions of the 48th Orthopaedic Research Society Meeting*, San Francisco, CA, March.
- [3] Lohmander, L. S., and Roos, H., 1994, "Knee Ligament Injury, Surgery and Osteoarthritis. Truth Or Consequences?," *Acta Orthop. Scand.*, **65**(6), pp. 605–609.
- [4] Gillquist, J., and Messner, K., 1999, "Anterior Cruciate Ligament Reconstruction and the Long-Term Incidence of Gonarthrosis," *Sports Med.*, **27**(3), pp. 143–156.
- [5] Fink, C., Hoser, C., Hackl, W., Navarro, R. A., and Benedetto, K. P., 2001, "Long-Term Outcome of Operative or Nonoperative Treatment of Anterior Cruciate Ligament Rupture—Is Sports Activity a Determining Variable?," *Int. J. Sports Med.*, **22**(4), pp. 304–309.

- [6] Jomha, N. M., Borton, D. C., Clingeleffer, A. J., and Pinczewski, L. A., 1999, "Long-Term Osteoarthritic Changes in Anterior Cruciate Ligament Reconstructed Knees," *Clin. Orthop. Relat. Res.*, **358**, pp. 188–193.
- [7] Beynnon, B., Howe, J. G., Pope, M. H., Johnson, R. J., and Fleming, B. C., 1992, "The Measurement of Anterior Cruciate Ligament Strain In Vivo," *Int. Orthop.*, **16**(1), pp. 1–12.
- [8] Henning, C. E., Lynch, M. A., and Glick, K. R., Jr., 1985, "An In Vivo Strain Gage Study of Elongation of the Anterior Cruciate Ligament," *Am. J. Sports Med.*, **13**(1), pp. 22–26.
- [9] Lewis, J. L., Lew, W. D., and Schmidt, J., 1982, "A Note on the Application and Evaluation of the Buckle Transducer for the Knee Ligament Force Measurement," *J. Biomech. Eng.*, **104**(2), pp. 125–128.
- [10] Fleming, B. C., Peura, G. D., and Beynnon, B. D., 2000, "Factors Influencing the Output of an Implantable Force Transducer," *J. Biomech.*, **33**(7), pp. 889–893.
- [11] Holden, J. P., Grood, E. S., Korvick, D. L., Cummings, J. F., Butler, D. L., and Bylski-Austrow, D. L., 1994, "In Vivo Forces in the Anterior Cruciate Ligament: Direct Measurements During Walking and Trotting in a Quadruped," *J. Biomech.*, **27**(5), pp. 517–526.
- [12] Fleming, B. C., and Beynnon, B. D., 2004, "In Vivo Measurement of Ligament/Tendon Strains and Forces: A Review," *Ann. Biomed. Eng.*, **32**(3), pp. 318–328.
- [13] Woo, S. L., Debski, R. E., Wong, E. K., Yagi, M., and Tarinelli, D., 1999, "Use of Robotic Technology for Diarthrodial Joint Research," *J. Sci. Med. Sport*, **2**(4), pp. 283–297.
- [14] Fujie, H., Mabuchi, K., Woo, S. L., Livesay, G. A., Arai, S., and Tsukamoto, Y., 1993, "The Use of Robotics Technology to Study Human Joint Kinematics: A New Methodology," *J. Biomech. Eng.*, **115**(3), pp. 211–217.
- [15] Fujie, H., Sekito, T., and Orita, A., 2004, "A Novel Robotic System for Joint Biomechanical Tests: Application to the Human Knee Joint," *J. Biomech. Eng.*, **126**(1), pp. 54–61.
- [16] Li, G., Most, E., Sultan, P. G., Schule, S., Zayontz, S., Park, S. E., and Rubash, H. E., 2004, "Knee Kinematics With a High-Flexion Posterior Stabilized Total Knee Prosthesis: An In Vitro Robotic Experimental Investigation," *J. Bone Jt. Surg., Am. Vol.*, **86-A**(8), pp. 1721–1729.
- [17] Ma, C. B., Janaushek, M. A., Vogrin, T. M., Rudy, T. W., Harner, C. D., and Woo, S. L., 2000, "Significance of Changes in the Reference Position for Measurements of Tibial Translation and Diagnosis of Cruciate Ligament Deficiency," *J. Orthop. Res.*, **18**(2), pp. 176–182.
- [18] Rudy, T. W., Livesay, G. A., Woo, S. L., and Fu, F. H., 1996, "A Combined Robotic/Universal Force Sensor Approach to Determine In Situ Forces of Knee Ligaments," *J. Biomech.*, **29**(10), pp. 1357–1360.
- [19] Hurschler, C., Wulker, N., Windhagen, H., Plumhoff, P., and Hellmers, N., 2001, "Medially Based Anterior Capsular Shift of the Glenohumeral Joint. Passive Range of Motion and Posterior Capsular Strain," *Am. J. Sports Med.*, **29**(3), pp. 346–353.
- [20] Petersen, W., Lenschow, S., Weimann, A., Strobel, M. J., Raschke, M. J., and Zantop, T., 2006, "Importance of Femoral Tunnel Placement in Double-Bundle Posterior Cruciate Ligament Reconstruction: Biomechanical Analysis Using a Robotic/Universal Force-Moment Sensor Testing System," *Am. J. Sports Med.*, **34**(3), pp. 456–463.
- [21] Tashman, S., and Anderst, W., 2003, "In-Vivo Measurement of Dynamic Joint Motion Using High Speed Biplane Radiography and CT: Application to Canine ACL Deficiency," *J. Biomech. Eng.*, **125**(2), pp. 238–245.
- [22] Li, G., Wuerz, T. H., and DeFrate, L. E., 2004, "Feasibility of Using Orthogonal Fluoroscopic Images to Measure In Vivo Joint Kinematics," *J. Biomech. Eng.*, **126**(2), pp. 314–318.
- [23] Andriacchi, T. P., Alexander, E. J., Toney, M. K., Dyrby, C., and Sum, J., 1998, "A Point Cluster Method for In Vivo Motion Analysis: Applied to a Study of Knee Kinematics," *J. Biomech. Eng.*, **120**(6), pp. 743–749.
- [24] Tapper, J. E., Ronsky, J. L., Powers, M. J., Sutherland, C., Majima, T., Frank, C. B., and Shrive, N. G., 2004, "In Vivo Measurement of the Dynamic 3-D Kinematics of the Ovine Stifle Joint," *J. Biomech. Eng.*, **126**(2), pp. 301–305.
- [25] Soderkvist, I., and Wedin, P. A., 1993, "Determining the Movements of the Skeleton Using Well-Configured Markers," *J. Biomech.*, **26**(12), pp. 1473–1477.
- [26] Vischer, P., and Clavel, R., 2000, "Argos: A Novel 3-Dof Parallel Wrist Mechanism," *Int. J. Robot. Res.*, **19**(1), pp. 5–8.
- [27] Slabaugh, G., 1999, "Computing Euler Angles From a Rotation Matrix," available from http://home.comcast.net/~greg_slabaugh/publications/euler.pdf